Copyright © 2014 Tech Science Press CMC, vol.43, no.3, pp.175-196, 2014

Modeling in Thermal Behavior of Charring Materials

Weijie Li[1], **Haiming Huang**[12], **Bangcheng Ai**[3] **and Ye Tian**[1]

Abstract: Physical and mathematical models are the key to analyze thermal behavior of charring materials in the thermal protection system of reentry vehicles subjected to aerodynamic heating. To explore the thermal behavior of charring ablator, we developed and compared two models (pyrolysis interface model and pyrolysis layer model) with pyrolysis and surface recession. Taking AVCOAT composites as an example, its nonlinear thermal behavior, which are caused by temperature dependent thermal properties, moving interfaces and moving boundary, were simulated using the calculation codes written respectively on the basis of the pyrolysis layer model and the pyrolysis interface model. Numerical results indicate that the nonlinear calculation is easier by the pyrolysis interface model than by the pyrolysis layer model; on the other hand, the selection of the pyrolysis interface temperature is complicated but significant in the calculation on thermal behavior of charring materials. This study will be helpful for the design of the thermal protection system in reentry vehicles.

Keywords: pyrolysis layer model, pyrolysis interface model, charring materials, pyrolysis interface temperature, thermal behavior.

1 Introduction

Charring materials may be used as a thermal protection system (TPS) for reentry vehicles subjected to high aerodynamic heat loads [Park (2007)]. At present, there have already been several typical charring ablators such as PICA and AVCOAT, which is an epoxy novolac resin with special additives in a fiberglass honeycomb. During the reentry of a manned spacecraft, charring materials operate heavily by absorbing heat through pyrolysis and rejecting it via pyrolysis gas injection back into the boundary layer of gas [Chen, Milos, Gokcen (2010)]. Furthermore, oxygen in the boundary layer of gas field may get to the ablation surface and then some car-

---

[1] Institute of Engineering Mechanics, Beijing Jiaotong University, Beijing, 100044, China.

[2] Corresponding author. E-mail: huanghaiming@tsinghua.org.cn

[3] China Academy of Aerospace Aerodynamics, Beijing, 100074, China.

bon on the surface at a high temperature is oxidized. Gradually, the ablation surface moves into inside the thermal protection layer [Suzuki, Sakai, Yamada (2007)]. Recently, many researchers have focused on simulations for the thermal response of charring materials [Stackpoole, Thornton (2010), Desai, Lawson, Keblinski (2011), Gibson, Browne, Feih (2012)]. Lattimer, Ouellette and Trelles (2011) used Arrhenius law to analyze in-depth temperature distribtution and measure the decomposition kinetic parameters. This method combines thermal analysis using tests with the heat conduction equations, but the test results depend heavily on the heating rate, which has great difference with that of reentry. Even, this method cannot observe the moving interfaces and boundary. While, the pyrolysis layer model can reflect the real situation. Usually, there are four layers such as the virgin layer, the pyrolysis layer, the char layer and the ablation layer in the pyrolysis layer model [Li, Huang, Tian (2015)]. Thermal properties of charring ablators changing all the time with pyrolysis were researched by both test and theoretical methods [Mouritz, Feih, Kandare (2009), Panescu, Whayne, Fleischman (1995), Park, Kwon, Wang (2014), Milos, Scott, Papa (2014)], and the heat conduction equations with moving boundaries or temperature dependent thermal properties are strong nonlinear [Johansson, Lesnic, Reeve (2014), Chang, Liu (2012), Hosseini, Shahmorad, Masoumi (2013), Duan, Rach, Wazwaz (2013), Henderson, Wiebelt, Tant (1985)]. In addition, the pyrolysis interface model regards the pyrolysis layer as an interface [Li, Huang, Zhang (2014)]. Regrettably, how to set the temperature at the pyrolysis interface has always been a controversial issue, because the temperature of the pyrolysis layer varies from 589K to 811K for AVCOAT composite [Curry, Stephens (1970), Williams, Curry (1992)]. Up to now, there are merely research on the comparison between the pyrolysis layer model and the pyrolysis interface model. An optimization approach to TPS in reentry vehicles remains a longstanding challenge. Toward this objective, we will simulate the nonlinear thermal behavior of AVCOAT composites by using the calculation codes respectively on the basis of the pyrolysis layer model and the pyrolysis interface model, and explore whether the pyrolysis interface temperature can affect on thermal behavior in this study.

2 Models

2.1 Physical models

The thermal protection performance of charring materials in TPS involves many complex physical and chemical processes. Typical charring composites contain carbon fiber and organic resin, which can be pyrolyzed and produce a condensed phase carbonaceous residue (called the char) when the resin is heated. The gases percolate through the porous char to the heated surface and simultaneously the flowing of pyrolysis gases also brings thermal blockage.

2.1.1 Pyrolysis layer model

Charring materials under heat flux absorb heat by the heat capacity of material itself and release a little heat by the surface radiation. When the surface temperature rises up to the beginning pyrolysis temperature T_{vp} of charring material, the resin in material on the surface starts to pyrolyze. Continuing heating, a char layer is forming on the surface when the surface temperature reaches the complete pyrolysis temperature T_{pc}. From now on, charring material transforms into an ablator with three layers. Heating continues, surface temperature reaches the surface recession temperature T_s, and the ablation surface gradually moves into inside the thermal protection layer.

We can develop a one-dimensional pyrolysis layer model (Fig. 1) since the temperature gradient vertically to the surface is much larger than those in the other orientations [Belghazi, Ganaoui, Labbe (2010), Huang, Xu, Huang (2014)]. Assume that: (1) pyrolysis gases do not react chemically with the porous char layer through which it flows; (2) there is no secondary cracking of pyrolysis gases. Thus, along the x direction, the ablator is divided into four layers, namely the virgin layer, the pyrolysis layer, the char layer and the ablation layer. In Fig. 1, q is the hot wall heat flux during reentry, x_{vp}, x_{pc} and x_s are coordinates of two moving interfaces and one moving boundary, L is the thickness of virgin materials without ablation.

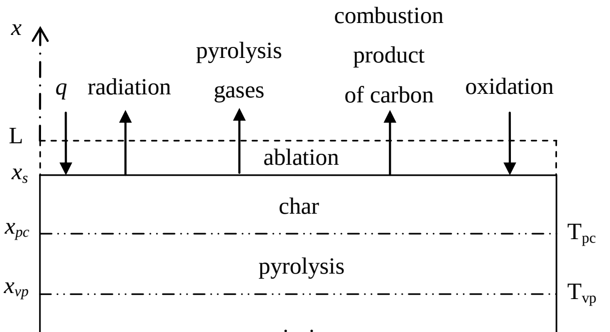

Figure 1: One-dimensional pyrolysis layer model.

The physical-chemical phenomena of the four layers are briefly introduced as follows

(1) The virgin layer: the temperature of material is lower than the beginning pyrolysis temperature.

(2) The pyrolysis layer: it is an unsteady and complex zone of ablator with two interfaces moving to the bondline. The temperature of interface between the virgin layer and the pyrolysis layer is a constant T_{vp}. The temperature of interface between the pyrolysis layer and the char layer is a constant T_{pc}. On the one hand, materials pyrolyze and release mixed gases which mainly consist of methane, ethylene, acetylene, hydrogen. On the other hand, foaming solid carbon forms continuously. Mechanism of absorbing heat can be concluded as ablator absorbing heat by pyrolysis, the heat capacities of solid carbon and pyrolysis gases absorbing heat. In addition, there exists the seepage of pyrolysis gas, the reactions between gas and solid and the change rate of density in this layer.

(3) The char layer: there is a solid carbon structure remained in the ablator above the temperature of material exceeding the complete pyrolysis temperature. During the pyrolysis gases flow through this layer to the surface of the ablator, solid carbon and pyrolysis gases continue to absorb thermal, and even the secondary cracking of pyrolysis gases is taken into consideration if necessary.

(4) The ablation layer: it is an extremely complex zone with both absorbing and releasing heat. For example, convection and radiation function directly on the surface of ablator; surface carbon reacts with oxygen; pyrolysis gases and combustion products of carbon inject to the boundary layer, which can change the velocity, temperature and concentration of gas.

2.1.2 *Pyrolysis interface model*

Assume that: (1) pyrolytic reaction only occurs on the pyrolysis interface which the pyrolysis layer between a char layer and a virgin material layer is simplified as. (2) pyrolysis gases do not react chemically with the porous char layer through which it flows [Li, Huang, Zhang (2014), Becker, Herwig (2013)]. In Fig. 2, x_{vc} is the coordinate of pyrolysis interface which is a function of time, T_{vc} is the constant temperature of pyrolysis interface. It is clearly that the pyrolysis interface model is a simplification of the pyrolysis layer model.

2.2 *Mathematical models*

2.2.1 *Pyrolysis layer model*

Based on the pyrolysis layer physical model, the transient heat conduction equations for pyrolysis layer model are respectively written in the forms

$$\rho_1 c_1 \frac{\partial T(x,t)}{\partial t} = \frac{\partial}{\partial x}[k_1 \frac{\partial T(x,t)}{\partial x}] \quad 0 \le x < x_{vp} \tag{1}$$

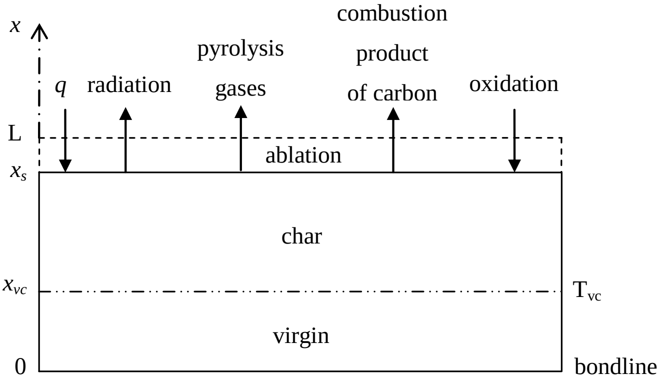

Figure 2: One-dimensional pyrolysis interface model.

$$\rho_2 c_2 \frac{\partial T(x,t)}{\partial t} = \frac{\partial}{\partial x}[k_2 \frac{\partial T(x,t)}{\partial x}] + \dot{m}_{g2} c_g \frac{\partial T(x,t)}{\partial x} + \frac{\partial \rho_2}{\partial t} \cdot \mathrm{h}_g \quad x_{vp} \le x < x_{pc} \tag{2}$$

$$\rho_3 c_3 \frac{\partial T(x,t)}{\partial t} = \frac{\partial}{\partial x}[k_3 \frac{\partial T(x,t)}{\partial x}] + \dot{m}_{g3} c_g \frac{\partial T(x,t)}{\partial x} \quad x_{pc} \le x \le x_s \tag{3}$$

where ρ, c and k are respectively the density, the specific heat and the thermal conductivity. $\dot{m}$ is the mass injection rate, and h is the enthalpy. The subscripts 1, 2, 3 and g represent the virgin layer, the pyrolysis layer, the char layer and pyrolysis gas, respectively.

If the accumulation of gases is ignored, the change of mass injection rate yields to the change of density. The conservation of mass may be denoted by [Gibson, Browne, Feih (2012)]

$$\frac{\partial \rho_2}{\partial t} = -\frac{d\dot{m}_{g2}}{dx} \tag{4}$$

$$\dot{m}_{g3} = \dot{m}_{g2}|_{x=x_c} \tag{5}$$

It is noteworthy that ρ_1 ,k_1, c_g, h and ρ_3 are constant values, while other coefficients of the above equations are functions of temperature. Noting that

$$\frac{\partial}{\partial x}[k_2 \frac{\partial T(x,t)}{\partial x}] = k_2 \frac{\partial^2 T(x,t)}{\partial x^2} + \frac{dk_2}{dT}[\frac{\partial T(x,t)}{\partial x}]^2 \tag{6}$$

$$\frac{\partial \rho_2}{\partial t} = \frac{d\rho_2}{dT} \cdot \frac{\partial T(x,t)}{\partial t} \tag{7}$$

$$\frac{\partial}{\partial x}[k_3 \frac{\partial T(x,t)}{\partial x}] = k_3 \frac{\partial^2 T(x,t)}{\partial x^2} + \frac{dk_3}{dT}[\frac{\partial T(x,t)}{\partial x}]^2 \tag{8}$$

and combining eqs.(6)-(8) with eqs.(1)-(3), we obtain the governing equations

$$\rho_1 c_1 \frac{\partial T(x,t)}{\partial t} = k_1 \frac{\partial^2 T(x,t)}{\partial x^2} \tag{9}$$

$$(\rho_2 c_2 - \frac{d\rho_2}{dT} \cdot \mathrm{h}_g)\frac{\partial T(x,t)}{\partial t} = k_2 \frac{\partial^2 T(x,t)}{\partial x^2} + \frac{dk_2}{dT}[\frac{\partial T(x,t)}{\partial x}]^2 + \dot{m}_{g2} c_g \frac{\partial T(x,t)}{\partial x} \tag{10}$$

$$\rho_3 c_3 \frac{\partial T(x,t)}{\partial t} = k_3 \frac{\partial^2 T(x,t)}{\partial x^2} + \frac{dk_3}{dT}[\frac{\partial T(x,t)}{\partial x}]^2 + \dot{m}_{g3} c_g \frac{\partial T(x,t)}{\partial x} \tag{11}$$

The nonlinear influence coming from the temperature dependent quadratic term in eq. (10) makes the calculation difficult.

Suppose that the bondline of ablator is adiabatic, so the boundary conditions are given by

$$-k_1 \frac{\partial T(x,t)}{\partial x} = 0 \quad x = 0 \tag{12}$$

$$T = \mathrm{T}_p \quad x = x_{vp} \tag{13}$$

$$T = \mathrm{T}_c \quad x = x_{pc} \tag{14}$$

$$-k_3 \frac{\partial T(x,t)}{\partial x} = \varphi q - \varepsilon \sigma T_w^4 + \dot{m}_{com} \mathrm{h}_{com} \quad x = x_s \tag{15}$$

where ε is the emissivity of the ablation surface, σ is Stefan-Boltzmann constant, and T_w is the surface temperature of ablator changing with time, thermal blockage coefficient φ is a number between 0 and 1 relating with mass injection rate, recovery enthalpy and cold wall heat flux q_{cold}, which can be write as

$$\varphi = 1 - 0.58(\dot{m}_{g3} + \dot{m}_{com})\frac{h_r}{q_{cold}} \tag{16}$$

where subscript *com* represents the combustion of surface carbon,h_r is the recovery enthalpy, which is the function of cold wall heat flux

$$h_r = 3 \times 10^{-5} q_{cold}^2 - 146 q_{cold} + 2 \times 10^8 \tag{17}$$

and the hot wall heat flux$q$ is given by [Potts (1995)]

$$q = q_{cold}(1 - \frac{h_w}{h_r}) \tag{18}$$

where h_w represents the wall enthalpy, which is the function of surface temperature

$$h_w = \begin{cases} 8.33 \times 10^2 T_w - 2.49 \times 10^5, & 300K \le T_w < 1500K \\ -5 \times 10^3 T_w + 8.5 \times 10^6, & 1500K \le T_w < 1700K \\ 1.54 \times 10^3 T_w - 2.61 \times 10^6, & 1700K \le T_w \le 3000K \end{cases} \tag{19}$$

On the basis of conservation of mass, mass injection rate of the combustion of surface carbon is denoted by

$$\dot{m}_{com} = \rho_3 \frac{\Delta x_s}{\Delta t} \tag{20}$$

where, Δx_s is the moving boundary distance for each time point, $\Delta x_s / \Delta t$ is the line ablation rate.

It should be also paid attention that the heat flux at two moving interfaces must satisfy

$$-k_1 \frac{\partial T(x,t)}{\partial x} = -k_2 \frac{\partial T(x,t)}{\partial x} \quad x = x_{vp} \tag{21}$$

$$-k_2 \frac{\partial T(x,t)}{\partial x} = -k_3 \frac{\partial T(x,t)}{\partial x} \quad x = x_{pc} \tag{22}$$

And initial condition is written in the form

$$T(x) = \mathrm{T}_0 \quad t = 0 \tag{23}$$

2.2.2 Pyrolysis interface model

Based on the pyrolysis interface physical model, the transient heat conduction equations for pyrolysis interface model are respectively written in the forms

$$\rho_1 c_1 \frac{\partial T(x,t)}{\partial t} = \frac{\partial}{\partial x}[k_1 \frac{\partial T(x,t)}{\partial x}] \quad 0 \leq x < x_{vc} \tag{24}$$

$$\rho_3 c_3 \frac{\partial T(x,t)}{\partial t} = \frac{\partial}{\partial x}[k_3 \frac{\partial T(x,t)}{\partial x}] + \dot{m}_{g3} c_g \frac{\partial T(x,t)}{\partial x} \quad x_{vc} \leq x \leq x_s \tag{25}$$

The boundary conditions are shown as

$$-k_1 \frac{\partial T(x,t)}{\partial x} = 0 \quad x = 0 \tag{26}$$

$$T = \mathrm{T_{VC}} \quad x = x_{vc} \tag{27}$$

$$-k_3 \frac{\partial T(x,t)}{\partial x} = \varphi q - \varepsilon \sigma T_w^4 + \dot{m}_{com} \mathrm{h_{com}} \quad x = x_s \tag{28}$$

In the above model, the pyrolysis temperature T_{vc} is a known constant on the interface instead of an interval in the pyrolysis layer. The energy balance equation in pyrolysis interface is given by the relation

$$-k_3 \frac{\partial T(x,t)}{\partial x} = -k_1 \frac{\partial T(x,t)}{\partial x} + \dot{m}_{g3} \mathrm{h}_g \quad x = x_s \tag{29}$$

The other parameters and initial condition are same with that in the pyrolysis layer model.

Both of the above mathematical models are strongly nonlinear with the temperature dependent thermal properties, moving interfaces and moving boundary, which make the calculation for thermal behavior difficult. However, comparing to the calculation of the pyrolysis layer model, this model only considers one moving interface without temperature dependent thermal properties in the complex pyrolysis layer, which make the nonlinear calculation easier.

3 Numerical approaches

3.1 Discrete format

To obtain the thermal behavior of ablator, it is necessary to discretize the transient heat conduction equations, boundary and initial conditions, and write a computer code. Here we adopt the central difference format in an implicit numerical method.

$$\frac{\partial T(x,t)}{\partial x} = \frac{T_{j+1}^n - T_{j-1}^n}{2\Delta x} \tag{30}$$

$$\frac{\partial T^2(x,t)}{\partial x^2} = \frac{T_{j+1}^n - 2T_j^n + T_{j-1}^n}{(\Delta x)^2} \tag{31}$$

$$\frac{\partial T(x,t)}{\partial t} = \frac{T_j^n - T_j^{n-1}}{\Delta t} \tag{32}$$

We use transient the eq. (10) in pyrolysis layer model to illustrate the discretization. The discretization of eqs. (9), (11), (24) and (25) are the same with the that of eq. (10). The temperature dependent quadratic term in the equation has to be discretized as

$$\frac{dk_2}{dT}\Big[\frac{\partial T(x,t)}{\partial x}\Big]^2 = \frac{dk_2}{dT}\cdot\frac{\partial T(x,t)}{\partial x}\cdot\frac{\partial T(x,t)}{\partial x} = \frac{dk_2}{dT}\cdot\frac{T_{j+1}^{n-1} - T_j^{n-1}}{\Delta x}\cdot\frac{T_{j+1}^n - T_{j-1}^n}{2\Delta x} \tag{33}$$

Combining with eqs.(30)-(32), eq.(10) can be transformed into

$$\begin{aligned}\frac{T_j^n - T_j^{n-1}}{\Delta t} =& \frac{k_{2,j}^n}{\rho_{2,j}^n c_{2,j}^n - \frac{d\rho_2}{dT}\cdot h_g}\frac{T_{j+1}^n - 2T_j^n + T_{j-1}^n}{(\Delta x)^2} \\ &+ \frac{\frac{dk_2}{dT}\frac{T_{j+1}^{n-1} - T_j^{n-1}}{\Delta x} + \dot{m}_{g2,j}^n c_g}{\rho_{2,j}^n c_{2,j}^n - \frac{d\rho_2}{dT}\cdot h_g}\frac{T_{j+1}^n - T_{j-1}^n}{2\Delta x}\end{aligned} \tag{34}$$

Introducing $r = \frac{k^n_{2,j}}{\rho^n_{2,j} c^n_{2,j} - \frac{d\rho_2}{dT} \cdot h_g} \frac{\Delta t}{(\Delta x)^2}$, $z = \frac{\frac{dk_2}{dT} \frac{T^{n-1}_{j+1} - T^{n-1}_j}{\Delta x} + \dot{m}^n_{g2,j} c_g}{\rho^n_{2,j} c^n_{2,j} - \frac{d\rho_2}{dT} \cdot h_g} \frac{\Delta t}{2\Delta x}$ and substituting r and z into eq. (34), we obtain the discrete format

$$T^n_j - T^{n-1}_j = r(T^n_{j+1} - 2T^n_j + T^n_{j-1}) + z(T^n_{j+1} - T^n_{j-1}) \tag{35}$$

Let $A = 1 + 2rB = r + z, C = r - zD = T^{n-1}_j$, eq. (35) becomes

$$T^n_j = \frac{B}{A - CP_{j-1}} T^n_{j+1} + \frac{CQ_{j-1} + D}{A - CP_{j-1}} \tag{36}$$

where $P_j = \frac{B}{A - CP_{j-1}}$, $Q_j = \frac{CQ_{j-1} + D}{A - CP_{j-1}}$.

According to eq. (4), the integral formula for mass injection rate of pyrolysis gas of adjacent space points can be written by

$$\dot{m}^n_{g2,j} = \int_{x_{vp}}^{x_j} \frac{\partial \rho_2}{\partial t} dx = \frac{d\rho_2}{dT} \int_{x_{vp}}^{x_j} \frac{\partial T}{\partial t} dx \tag{37}$$

$$\dot{m}^n_{g2,j+1} = \int_{x_{vp}}^{x_{j+1}} \frac{\partial \rho_2}{\partial t} dx = \frac{d\rho_2}{dT} \int_{x_{vp}}^{x_{j+1}} \frac{\partial T}{\partial t} dx \tag{38}$$

Substitute eq. (37) into eq. (38), we can obtain the iterative formula of mass injection rate for j space point

$$\dot{m}^n_{g2,j} = \dot{m}^n_{g2,j+1} + \frac{d\rho_2}{dT} \int_{x_{j+1}}^{x_j} \frac{\partial T}{\partial t} dx \tag{39}$$

Transforming eq.(10) into

$$\frac{\partial T(x,t)}{\partial t} = \frac{1}{\rho_2 c_2 - \frac{d\rho_2}{dT} \cdot h_g} \{ k_2 \frac{\partial^2 T(x,t)}{\partial x^2} + \frac{dk_2}{dT} [\frac{\partial T(x,t)}{\partial x}]^2 + \dot{m}_{g2} c_g \frac{\partial T(x,t)}{\partial x} \} \tag{40}$$

and combining eq. (39), on the basis of Newton-Cotes equation, we can get the mass injection rate of pyrolysis gas for j space point

$$\begin{aligned} m^n_{g2,j} = & m^n_{g2,j+1} - \frac{d\rho_2}{dT} \cdot \frac{dx}{2} \cdot [\frac{k^n_{2,j} \frac{T^n_{j+1} - 2T^n_j + T^n_{j-1}}{(\Delta x)^2} + \frac{dk_2}{dT} (\frac{T^n_{j+1} - T^n_{j-1}}{2\Delta x}) + m^n_{g2,j} c_g \frac{T^n_{j+1} - T^n_{j-1}}{2\Delta x}}{\rho^n_{2,j} c^n_{2,j} - \frac{d\rho_2}{dT} \cdot h_g} \\ & + \frac{k^n_{2,j+1} \frac{T^n_{j+2} - 2T^n_{j+1} + T^n_j}{(\Delta x)^2} + \frac{dk_2}{dT} (\frac{T^n_{j+2} - T^n_j}{2\Delta x}) + m^n_{g2,j+1} c_g \frac{T^n_{j+2} - T^n_j}{2\Delta x}}{\rho^n_{2,j+1} c^n_{2,j+1} - \frac{d\rho_2}{dT} \cdot h_g}] \end{aligned} \tag{41}$$

3.2 Nonlinear analysis at moving interfaces

To calculate the thermal behavior of ablator in numerical simulation for two models, we have to know moving distance Δx_s of boundary, moving distancesΔx_{vp} andΔx_{pc} or $\Delta x_{vc}$of interfaces for each time point. Reference [Curry, Stephens (1970)] provided the surface recession rate of AVCOAT composite on the basis of reaction-rate-control regime (Fig. 3).

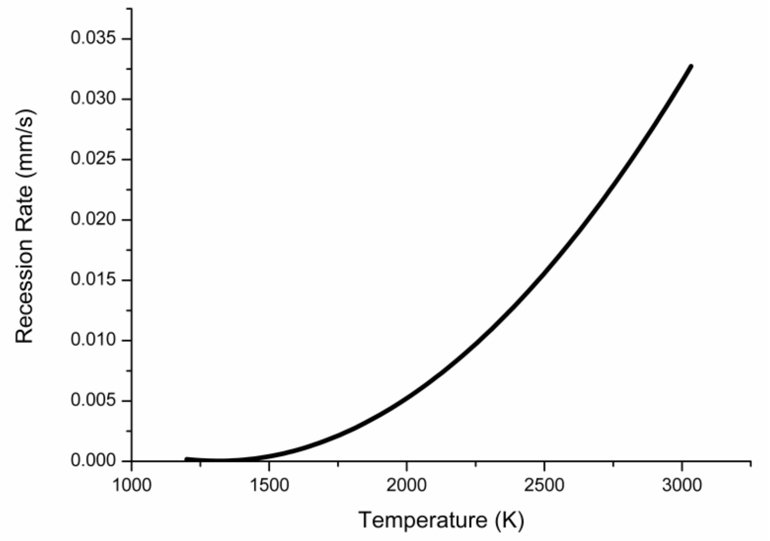

Figure 3: Surface recession rate vs. temperature.

To illustrate solutions for nonlinear effect by moving interfaces, we present the method for obtaining moving distances of interfaces in pyrolysis layer model for example. The nonlinear analysis at the moving interface of pyrolysis interface model is same with which we denote as follows.

Combining with eq. (20) with the surface recession rate in Fig. 3, we can get the mass injection rate of combustion of surface carbon in each time point. It depends strongly on surface temperature and influences in-depth temperature distribution, then affects seriously on moving interfaces distances.

Eqs. (21) and (22) can be used to calculate moving interfaces distances combining with eqs. (9)-(23). We compute the moving interfaces distances by Newton Secant method [Gibson, Browne, Feih (2012)], which is an iterative method.

Firstly, introduce two functions representing the heat flux difference on both sides of moving interfaces $x = x_{vp}$ and $x = x_{pc}$, respectively

$$F_{vp}(\Delta x_{vp}, \Delta x_{pc}) = -k_1 \frac{\partial T(x,t)}{\partial x} - [-k_2 \frac{\partial T(x,t)}{\partial x}] \quad x = x_{vp} \tag{42}$$

$$F_{pc}(\Delta x_{vp}, \Delta x_{pc}) = -k_2 \frac{\partial T(x,t)}{\partial x} - [-k_3 \frac{\partial T(x,t)}{\partial x}] \quad x = x_{pc} \tag{43}$$

where F_{vp} and F_{pc} represent the heat flux differences at two interfaces, which can be calculated combining with eqs. (9)-(23).

Then, for the sake of getting partial derivatives of function F_{vp} and F_{pc}, which depend on in-depth temperature distribution and changing thermal properties and cannot be calculated directly. We have to suppose two different initial moving distances at each interface. For Δx_{vp}, the initial values are Δx_{vp}^{0} and Δx_{vp}^{00}. Simultaneously, the initial values are Δx_{pc}^{0} and Δx_{pc}^{00} for Δx_{pc}. To calculate the roots Δx_{vp} and Δx_{pc} of eqs. (42) and (43), a matrix can be determined by the relation

$$\begin{bmatrix} \frac{F_{vp}(\Delta x_{vp}^{00}, \Delta x_{pc}^{0}) - F_{vp}(\Delta x_{vp}^{0}, \Delta x_{pc}^{0})}{\Delta x_{vp}^{00} - \Delta x_{vp}^{0}} & \frac{F_{vp}(\Delta x_{vp}^{0}, \Delta x_{pc}^{00}) - F_{vp}(\Delta x_{vp}^{0}, \Delta x_{pc}^{0})}{\Delta x_{pc}^{00} - \Delta x_{pc}^{0}} \\ \frac{F_{pc}(\Delta x_{vp}^{00}, \Delta x_{pc}^{0}) - F_{pc}(\Delta x_{vp}^{0}, \Delta x_{pc}^{0})}{\Delta x_{vp}^{00} - \Delta x_{vp}^{0}} & \frac{F_{pc}(\Delta x_{vp}^{0}, \Delta x_{pc}^{00}) - F_{pc}(\Delta x_{vp}^{0}, \Delta x_{pc}^{0})}{\Delta x_{pc}^{00} - \Delta x_{pc}^{0}} \end{bmatrix} \cdot \begin{bmatrix} \Delta x_{vp} - \Delta x_{vp}^{00} \\ \Delta x_{pc} - \Delta x_{pc}^{00} \end{bmatrix}$$
$$= \begin{bmatrix} F_{vp}(\Delta x_{vp}^{00}, \Delta x_{pc}^{00}) \\ F_{pc}(\Delta x_{vp}^{00}, \Delta x_{pc}^{00}) \end{bmatrix} \tag{44}$$

Obviously, from eq. (44) Δx_{vp} and Δx_{pc} can be obtained by the procedure of Newton Secant method shown as follows

1. Suppose initial values Δx_{vp}^{i}, Δx_{pc}^{j}. (i=0,00; j=0,00)
2. Combining with eqs. (9)-(23), calculate $F_{vp}(\Delta x_{vp}^{i}, \Delta x_{pc}^{j})$, $F_{pc}(\Delta x_{vp}^{i}, \Delta x_{pc}^{j})$ and eq. (44).
3. If $\left\| \begin{matrix} \Delta x_{vp} - \Delta x_{vp}^{00} \\ \Delta x_{pc} - \Delta x_{pc}^{00} \end{matrix} \right\|_{\infty} < \delta$, stop the iteration. δ is the permissible error. However, if $\left\| \begin{matrix} \Delta x_{vp} - \Delta x_{vp}^{00} \\ \Delta x_{pc} - \Delta x_{pc}^{00} \end{matrix} \right\|_{\infty} \geq \delta$, go to step (4).
4. If iteration times exceed a preset value, the method is a failure. Conversely, let $\Delta x_{vp}^{0} = \Delta x_{vp}^{00}$, $\Delta x_{pc}^{0} = \Delta x_{pc}^{00}$ and $\Delta x_{vp}^{00} = \Delta x_{vp}$, $\Delta x_{pc}^{00} = \Delta x_{pc}$, returning step (2) to begin iteration again.

The moving distances of interfaces and boundary can be calculated by methods mentioned above. According to eqs.(9-23), we can write a computer code to calculate the thermal behavior of ablator with pyrolysis layer model. In the same manner, we can also get the way to calculate the thermal behavior with pyrolysis interface model.

4 Numerical example

Taking AVCOAT composites as an example, its nonlinear thermal behavior is simulated using the calculation codes written respectively on the basis of the pyrolysis layer model and the pyrolysis interface model.

4.1 Material property parameters

4.1.1 Property parameters in the virgin layer and the char layer

Properties in the virgin layer and the char layer can be measured by experiments [Curry, Stephens (1970); Curry (1965)]. In these two layers, it is considered that the some property parameters (e.g. densities, thermal conductivity of the virgin layer, enthalpy of thermal decomposition and combustion of surface carbon, the specific heat of pyrolysis gas, the beginning pyrolysis temperature, the beginning carbonization temperature, the emissivity of ablation surface and Stefan-Boltzmann constant) are constants, and the other property parameter are functions of temperature [Curry, Stephens (1970); Williams, Curry (1992)], which are shown in Tabs 1-4.

Table 1: Property parameters as constants.

ρ_1	ρ_3	c_g	k_1	ε	σ	h_g	h_{com}
[kg/m^3]	[kg/m^3]	[J·kg^{-1}·K^{-1}]	[W·m^{-1}·K^{-1}]		[W·m^{-2}·K^{-4}]	[J/kg^3]	[J/kg^3]
512.59	320.37	2093	0.242	0.65	5.67×10^{-8}	8.77×10^{7}	1.163×10^{7}
T_0	T_{vp}	T_{pc}	T_s				
[K]	[K]	[K]	[K]				
300	589	811	1242				

Table 2: Specific heat of the virgin layer.

Temperature	Specific heat
[K]	[J·kg^{-1}·K^{-1}]
311	1457
367	1465
422	1549
478	1591
533	1758
589	1842

Table 3: Specific heat of the char layer.

Temperature	Specific heat
[K]	[J·kg^{-1}·K^{-1}]
811	1549
1367	1725
2756	1725
3033	1926

Table 4: Thermal conductivity of the char layer.

Temperature	Thermal conductivity
[K]	[W·m^{-1}·K^{-1}]
922	0.242
1033	0.381
1256	0.614
1367	0.736
1589	0.935
1700	1.030
1922	1.212

4.1.2 Property parameters in the pyrolysis layer

To get the thermal behavior with pyrolysis layer model, we have to know the thermal properties in pyrolysis layer. Thermal properties of the ablator in the pyrolysis layer are temperature dependent. It is proved that dealing with the thermal properties in the virgin layer and the char layer with linear interpolation is reasonable in calculation [Curry (1965)]. The thermal properties in the pyrolysis layer are

$$\rho_2 = \rho_1 - (\rho_1 - \rho_3)\cdot\left(\frac{T - T_{vp}}{T_{pc} - T_{vp}}\right) = -0.8659T + 1.0226\times 10^3[\mathrm{kg/m^3}] \tag{45}$$

$$\begin{aligned} c_2 &= c_1|_{x=x_{vp}} - (c_1|_{x=x_{vp}} - c_3|_{x=x_{pc}})\cdot\left(\frac{T - T_{vp}}{T_{pc} - T_{vp}}\right) \\ &= -0.994T + 2.3947\times 10^3[\mathrm{J\cdot kg^{-1}\cdot K^{-1}}] \end{aligned} \tag{46}$$

$$\begin{aligned} k_2 &= k_1|_{x=x_{vp}} - (k_1|_{x=x_{vp}} - k_3|_{x=x_{pc}})\cdot\left(\frac{T - T_{vp}}{T_{pc} - T_{vp}}\right) \\ &= 6.0988\times 10^{-5}T + 0.206[\mathrm{W\cdot m^{-1}\cdot K^{-1}}] \end{aligned} \tag{47}$$

4.2 Calculation conditions

Assume constant heat flux 8.79×10^5W/m^2 at the surface, L=15mm, heating time 100s for each model. We set T_{vc}=589K, 630K, 680K, 730K, 770K and 811K in pyrolysis interface model and then compare their calculation results with that of pyrolysis layer model, where 589K and 811K is respectively the beginning and complete pyrolysis temperature.

4.3 Results and discussions

Based on the pyrolysis layer model and the pyrolysis interface model, nonlinear thermal behavior of AVCOAT composites obtained is shown in Figs. 4 - 9.

From Fig. 4, we can know that the bondline temperature for each model stays at a temperature 300K in initial 25s. Then they rise smoothly. The bondline temperature history of the pyrolysis interface model except T_{vc}=589K is larger than that of the pyrolysis layer model. The bondline temperature history of the pyrolysis interface model (T_{vc}=630K) is the most close to that of the pyrolysis layer model. With T_{vc} increasing, the bondline temperature history of the correspongding pyrolysis interface model increases. And the bondline temperature history of the pyrolysis interface model (T_{vc}=811K) is the largest of all. It is obvious that the pyrolysis interface temperature greatly affect the calculation results of bondline temperature history.

It is well known that the bondline temperature is the key to evaluate the performance of TPS. As the results shown in Fig. 4, we will get a conservative calcualtion results when setting T_{vc}=811K in the pyrolysis interface model. However, TPS will be in a danger situation when setting T_{vc}=589K in the pyrolysis interface model.

The surface temperature for each model can be seen in Fig. 5. In the first 40s, all curves rise rapidly. After that, they tend to be stable because of the constant heat flux on the surface. The severe oscillation in the curve of pyrolysis layer model at the beginning comes from the occurrence of pyrolysis layer. Other oscillations of pyrolysis layer model are affected by the nonlinear calculation for the moving distances of moving interfaces. The surface temperature of pyrolysis layer model is a little larger than that of pyrolysis interface models except T_{vc}=811K. The surface temperature history of the pyrolysis interface model (T_{vc}=811K) is the largest of all and agrees very well with that of the pyrolysis layer model. With T_{vc} increasing, the surface temperature of the corresponding pyrolysis interface model increases. The surface temperature history of the pyrolysis interface model (T_{vc}=589K) is the smallest of all. So we can know that the pyrolysis interface temperature has severe influence on the calculation results of surface temperature history.

Fig. 6 shows the thickness of surface recession for each model. In the first 20s,

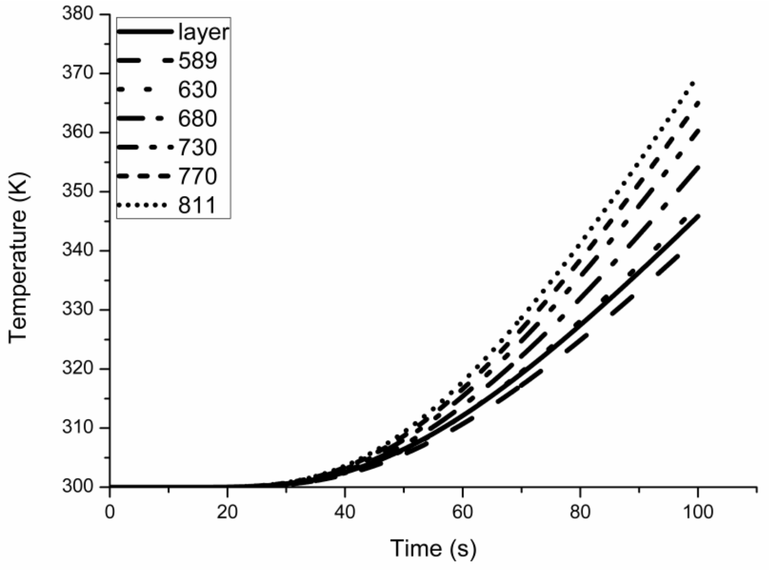

Figure 4: Bondline temperature history.

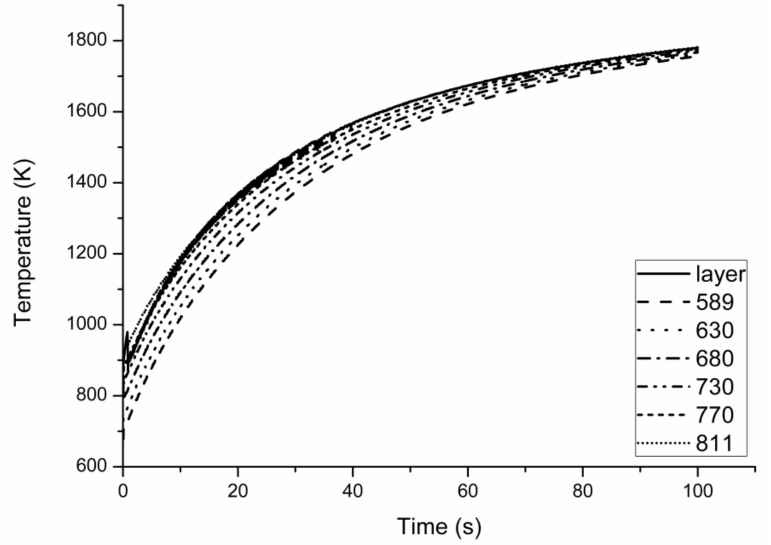

Figure 5: Surface temperature history.

surface recession of each model does not begin. After that, the thickness of pyrolysis layer model is a little larger than that of pyrolysis interface models except T_{vc}=811K. The thickness of surface recession for the pyrolysis interface model (T_{vc}=589K) is the smallest of all. With T_{vc} increasing, the thickness of surface recession for the corresponding pyrolysis interface model increases. The thickness of surface recession for the pyrolysis interface model (T_{vc}=811K) is the largest of all and in excellent agreement with that for the pyrolysis layer model. It can be seen that the pyrolysis interface temperature has severe influence on the calculation results of surface recession thickness.

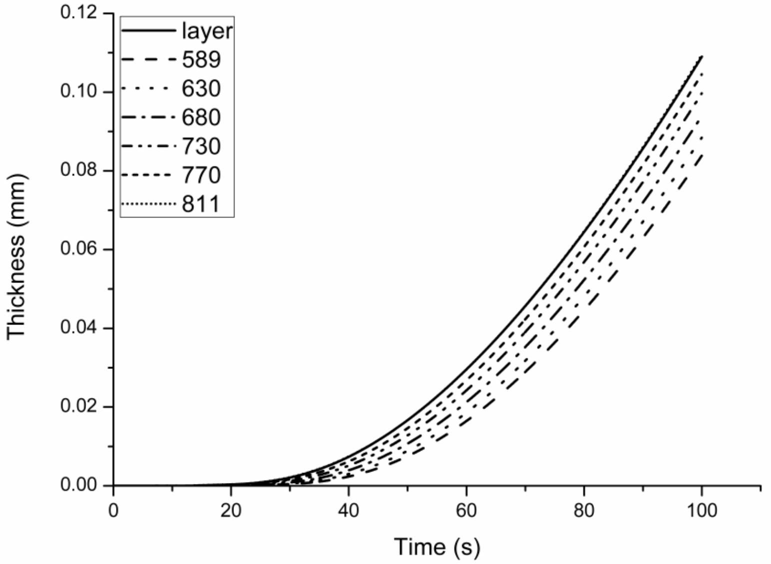

Figure 6: Surface recession thickness history.

The thickness of the char layer for each model is shown in Fig. 7. The occurrence of the char layer of the pyrolysis interface models is earlier than that of the pyrolysis layer model. After 10s, the char layer thickness of pyrolysis layer model always exceeds that of pyrolysis interface model except T_{vc}=589K. The char layer thickness of the pyrolysis interface model (T_{vc}=589K) is the largest of all. With T_{vc} increasing, the thickness of the char layer of the corresponding pyrolysis interface model decreases. The char layer thickness of the pyrolysis interface model (T_{vc}=811K) is the smallest of all. However, the char layer thickness of the pyrolysis interface model (T_{vc}=630K) is consistent with that of the pyrolysis layer model.

The mass injection rate in the char layer for each model can be seen in Fig. 8. As seen in Fig. 8, the curves are very close to each other with oscillations which

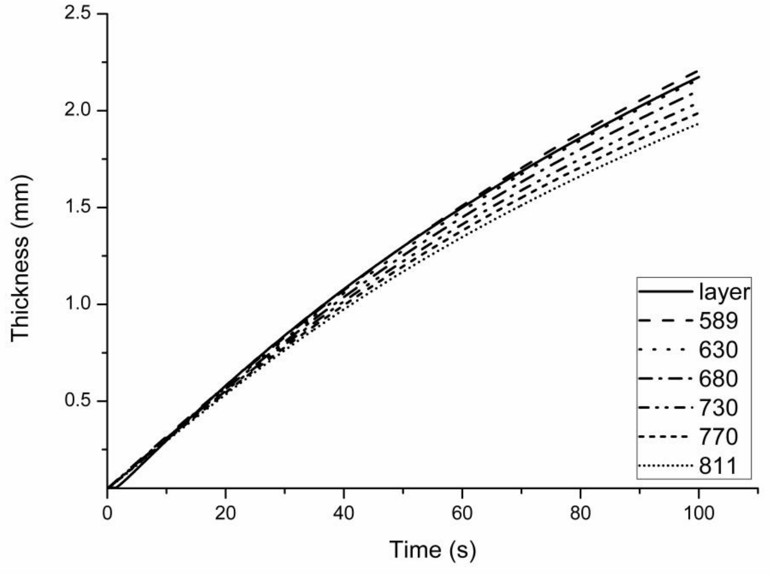

Figure 7: Thickness history of char layer.

caused by nonlinear calculation of moving interfaces. In order to identify the curves clearly, the local position is zoomed in Fig. 8. All curves increase in initial time and then decrease. The mass injection rate of the pyrolysis layer model is the largest in the first 10s, then begins to decrease crossing with that of the pyrolysis interface models. In the end, the mass injection rate of the pyrolysis interface model (T_{vc}=589K) is the largest of all. The mass injection rate of the pyrolysis layer model is the smallest of all. The mass injection rate of the pyrolysis interface model (T_{vc}=811K) is closest to that of the pyrolysis layer model. So, the pyrolysis interface temperature has effect on the calculation results of mass injection rate.

As shown in Fig. 9, we can see the in-depth temperature distribution for each model. The temperature distribution of the pyrolysis interface model consists of two stages. The discontinuous point in the curve of pyrolysis interface model is the interface between the virgin layer and the char layer. The temperature at this point is T_{vc} which can be seen clearly. The curve corresponding to the pyrolysis layer model is smoother than the pyrolysis interface curve. From this curve, we can see that the temperature distribution consists of three stages—the virgin layer, the pyrolysis layer and the char layer. The pyrolysis layer is thin. And the temperature of the beginning and end of this layer corresponds to T_{vp} and T_{pc}, respectively. We can also know that the temperature in the virgin layer of pyrolysis interface model except T_{vc}=589K is larger than that of pyrolysis layer model. However, the temper-

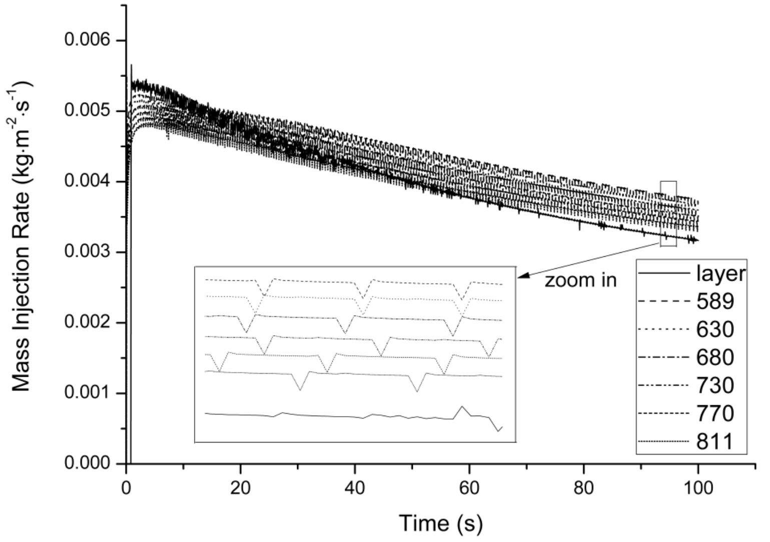

Figure 8: Mass injection rate history in the char layer.

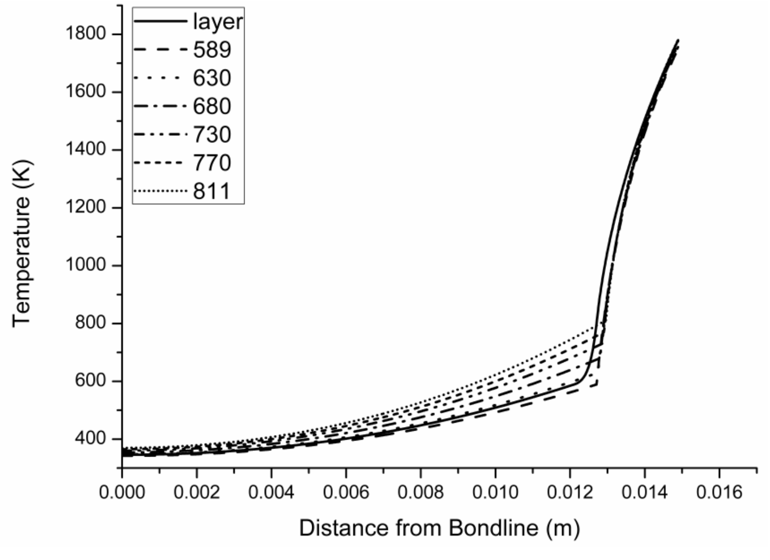

Figure 9: In-depth temperature distribution at 100s.

ature in the char layer of pyrolysis interface model is close to that of pyrolysis layer model. The temperature distribution of the pyrolysis interface model (T_{vc}=630K) is in accordance with that of the pyrolysis layer model. It is concluded that the pyrolysis interface temperature has severe influence on the calculation results of in-depth temperature distribution.

5 Conclusions

Two models—pyrolysis interface model and pyrolysis layer model were developed and compared in thermal behavior of charring ablators. Taking AVCOAT composites as an example, its thermal behavior was calculated by the computer codes written. From the numerical results, it can be concluded as follows:

1. The nonlinear calculation in thermal behavior of charring ablator is easier by the pyrolysis interface model than by the pyrolysis layer model. The pyrolysis interface model concludes only one moving interface and ignores the changing thermal properties in the pyrolysis layer.
2. The selection of the pyrolysis interface temperature is complicated but significant in the calculation on the thermal behavior. What is more, setting T_{vc}=630K in the pyrolysis interface model is more reasonable when designing a TPS material for vehicle reentry.

Acknowledgement: This work was supported by the National Natural Sciences Foundation of China (11472037, 11272042) and the Project of Education Ministry of China (62501036026).

Nomenclature

ρ	density [kg/m^3]
c	specific heat [J·kg^{-1}·K^{-1}]
k	thermal conductivity [W·m^{-1}·K^{-1}]
$\dot{m}$	mass injection rate [kg·m^{-2}·s^{-1}]
h	enthalpy [J/kg]
q	heat flux [W/m^2]
ε	emissivity of ablation surface
σ	Stefan-Boltzmann constant[W·m^{-2}·K^{-4}]
T	temperature [K]
L	thickness of charring ablator [m]
x	space coordinate [m]

t	time [s]
F	heat flux difference [W/m^2]

Subscripts

1	virgin
2	pyrolysis layer
3	char
vp	interface between the virgin layer and the pyrolysis layer
pc	interface between the pyrolysis layer and the char layer
vc	interface between the virgin layer and the char layer
s	surface ablation
g	pyrolysis gas
cold	cold wall
w	surface
r	recovery
com	combustion

Superscripts

i	initial value of Newton Secant method for interface between the virgin layer and the pyrolysis layer
j	initial value of Newton Secant method for interface between the pyrolysis layer and the char layer

References

Becker, S. M.; Herwig, H. (2013): One Dimensional Transient Heat Conduction in Segmented Fin-Like Geometries with Distinct Discrete Peripheral Convection. *Int. J. Therm. Sci.*, vol. 71, no. 1, pp. 148-162.

Belghazi, H.; Ganaoui, M.; Labbe, J. C. (2010): Analytical Solution of Unsteady Heat Conduction in A Two-Layered Material in Imperfect Contact Subjected to A Moving Heat Source. *Int. J. Therm. Sci.*, vol. 49, no. 2, pp. 311-318.

Chang, C. W.; Liu, C. S. (2012): A New Optimal Scheme for Solving Nonlinear Heat Conduction Problems. *CMES*, vol. 88, no. 4, pp. 269-291.

Chen, Y. K.; Milos, F. S.; Gokcen, T. (2010): Loosely Coupled Simulation for Two-Dimensional Ablation and Shape Change. *J. Spacecraft Rockets*, vol. 47, no. 5, pp. 775-785.

Curry, D. M. (1965): An Analysis of A Charring Ablation Thermal Protection System. NASA-TN-D-3150.

Curry, D. M.; Stephens, E. W. (1970): *Apollo Ablator Thermal Performance at Superorbital Entry Velocities*. National Aeronautics and Space Administration.

Desai, T. G.; Lawson, J. W.; Keblinski, P. (2011): Modeling Initial Stage of Phenolic Pyrolysis: Graphitic Precursor Formation and Interfacial Effects. *Polymer*, vol. 52, no. 2, pp. 577-585.

Duan, J. S.; Rach, R.; Wazwaz, A. M. (2013): A New Modified Adomian Decomposition Method for Higher-Order Nonlinear Dynamical Systems. *CMES*, vol. 94, no. 1, pp. 77-118.

Gibson, A. G.; Browne, T. N. A.; Feih, S. (2012): Modeling Composite High Temperature Behavior and Fire Response under Load. J. Compos. Mater., vol. 46, no. 16, pp. 2005-2022.

Henderson, J. B.; Wiebelt, J. A.; Tant, M. R. (1985): A Model for The Thermal Response of Polymer Composite Materials with Experimental Verification. *J. Compos. Mater.*, vol. 19, no. 6, pp. 579-595.

Hosseini, S. A.; Shahmorad, S.; Masoumi, H. (2013): Extension of The Operational Tau Method for Solving 1-D Nonlinear Transient Heat Conduction Equations. *J. King Saud University-Sci.*, vol. 25, no. 4, pp. 283-288.

Huang, H. M.; Li, W. J.; Yu, H. L. (2014): Thermal Analysis of Charring Materials based on Pyrolysis Interface Model. *Therm. Sci.*, vol. 18, no. 5, pp. 1583-1588.

Johansson, B. T.; Lesnic, D.; Reeve, T. (2014): A Meshless Method for An Inverse Two-Phase One-Dimensional Nonlinear Stefan Problem. *Math. Comput. Simulat.*, vol. 101, pp. 61-77.

Lattimer, B. Y.; Ouellette, J.; Trelles, J. (2011): Thermal Response of Composite Materials to Elevated Temperatures. *Fire. Technol.*, vol. 47, no. 4, pp. 823-850.

Li, W. J.; Huang, H. M.; Zhang, Z. M. (2014): Effects of Gradient Density on Thermal Protection Performance of Avcoat Composites under Varied Heat Flux. *Polym. Composite.*, DOI 10.1002/pc.23263.

Li, W. J.; Huang, H. M.; Tian, Y. (2015): Nonlinear Analysis on Thermal Behavior of Charring Materials with Surface Ablation. *Int. J. Heat Mass Tran.*, http://dx.doi.org/10.1016/j.ijheatmasstransfer.2015.01.004.

Milos, F. S.; Scott, C. D.; Papa, S. V. Del. (2014): Arcjet Testing and Thermal Model Development for Multilayer Felt Reusable Surface Insulation. *J. Spacecraft. Rockets*, vol. 51, no. 2, pp. 397-411.

Mouritz, A. P.; Feih, S.; Kandare, E. (2009): Review of Fire Structural Modelling of Polymer Composites. *Compos. Part A-Appl. S.*, vol. 40, no. 12, pp. 1800-1814.

Panescu, D.; Whayne, J. G.; Fleischman, S. D. (1995): Three-Dimensional Finite Element Analysis of Current Density and Temperature Distributions during Radio-Frequency Ablation. *IEEE. T. Bio-Med. Eng.*, vol. 42, no. 9, pp. 879-890.

Park, C. (2007): Calculation of Stagnation-Point Heating Rates Associated with Stardust Vehicle. *J. Spacecraft Rockets*, vol. 44, no. 1, pp. 24-32.

Park, J. M.; Kwon, D. J.; Wang, Z. J. (2014): Effects of Carbon Nanotubes and Carbon Fiber Reinforcements on Thermal Conductivity and Ablation Properties of Carbon/Phenolic Composites. *Compos. Part B-Eng.*, vol. 67, pp. 22-29.

Potts, R. L. (1995): Application of Integral Methods to Ablation Charring Erosion-A Review. *J. Spacecraft Rockets*, vol. 32, no. 2, pp. 200-209.

Stackpoole, M.; Thornton, J. (2010): Ongoing TPS Development at NASA Ames Research Center. *ERC lnc., NASA Ames Research Center, Moffett Field CA*, ARC-E-DAA-TN2373.

Suzuki, T.; Sakai, T.; Yamada, T. (2007): Calculation of Thermal Response of Ablator under Arcjet Flow Condition. *J. Thermophys. Heat Tr.*, vol. 21, no. 2, pp. 257-266.

Williams, S. D.; Curry, D.M. (1992): Thermal Protection Materials: Thermophysical Property Data. *NASA STI/Recon Technical Report N*, Report/Patent Number: NASA-RP-1289, S-693, NASA 1.61:1289.